RESEARCH PAPER

CrossMark

On repair weld residual stresses and significance to structural integrity

Pingsha Dong [1,2]

Abstract

This paper starts with a brief state of the art assessment on what has been learned over the last few decades in understanding residual stress development mechanisms, particularly those uniquely associated with weld repairs. A special emphasis will be given to how some of the residual stress features contribute to structural integrity of a component containing weld repairs. In contrast to initial fabrication welds, residual stresses associated with finite length repair welds tend to exhibit important invariant features, regardless of component configurations, materials, and to some degree, welding procedures. Such invariant features are associated with the severe restraint conditions present in typical repair situations. A number of weld repair cases are examined in this paper. In addition to highlighting important residual stress distribution features, fracture mechanics calculations are performed to examine how repair weld residual stresses quantitatively contribute to crack driving force as a function of crack location and size. One simple and effective technique for mitigating detrimental residual stress effects on structural integrity is also demonstrated by considering overall weld repair dimensions.

1 Introduction

Over the last two decades, there has been a growing interest in residual stresses caused by weld repairs and their proper treatment in fitness-for-service (FFS) assessment of engineering structures and equipment either during construction or in service [1–9]. During construction, weld repairs may be introduced to mend manufacturing quality deviations from relevant construction Codes and Standards (e.g., [10–12]). During service, structures or equipment may experience certain damages that require weld repairs to ensure that original design lives can still be achieved or further extended for maximizing

investment returns. The latter has become an increasingly important research topic of late, in which a recommended weld repair procedure may be required for effectively mitigating repair weld residual stress effects on structural integrity [1, 2]. This is because it has been well established that weld repairs can introduce much more significant residual stresses to a component than initial welds due to more severe restraint conditions in repair welds than initial welds [1, 2, 13, 14]. As a case in point, Fig. 1 shows a well-documented example on repair weld effects on AL 2195 wide panel strength tests (see Fig. 1a), comparing photo-strain distributions between two test panels under the same remote tension loading of 14 Ksi (97 MPa) [1, 2]. The panel with only initial weld (see Fig. 1b) shows barely noticeable straining within weld fusion zone. In contrast, the test panel with a weld repair as indicated in Fig. 1c under the same remote loading conditions shows a rather high level of straining accumulated within the entire repair weld region, resulting in about 30–40% strength reduction in wide panel test results [2].

Therefore, an improved understanding of residual stress development mechanisms uniquely associated with weld repairs, and their effects on structural integrity become critically important. There have been numerous investigations
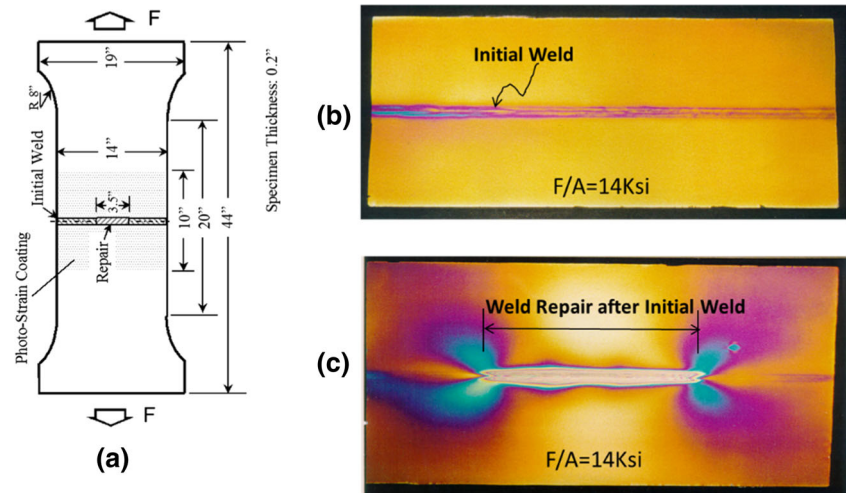

✉ Pingsha Dong
  dongp@umich.edu

1   Department of Naval Architecture and Marine Engineering, University of Michigan, Ann Arbor, MI 48109, USA

2   Department of Mechanical Engineering, University of Michigan, Ann Arbor, MI 48109, USA

employing various residual stress measurement techniques
(e.g., [1–4]) and finite element modeling methods (e.g., [1,
5–9]) for characterizing residual stresses for weld repairs in
various structural configurations, as well as treatment of such
residual stresses in fracture assessment models. To a large
extent, there has been a general agreement among most re-
searchers that residual stresses caused by weld repairs play a
much more important role to structural integrity management
than those by initial welds [2–4, 13–15] and must be properly
taken into account when performing fitness for service
assessment.

However, assessment procedures given by major FFS
Codes and Standards such as BS7910 [10], R6 [11], and
API 579 RP-1/ASME FFS-1 [12] provide rather limited guid-
ance on residual stress profiles relevant to various repair con-
ditions and how to treat repair weld residual stresses under
repair conditions, as reviewed by Dong et al. [16]. Residual
stress prescriptions in these procedures were based on inter-
pretations of experimental measurements on selected compo-
nents and/or available finite element residual stress solutions
with a level of conservatism being built-in (e.g., [3, 4]).
Without clearly establishing key controlling parameters, it is
difficult to extend some of the empirical findings obtained
from one set of repair conditions to others. Unlike initial fab-
rication welds, residual stresses in weld repairs tend to exhibit
strong three-dimensional (3D) features that are strongly de-
pendent upon repair weld dimensions in addition to compo-
nent geometry and welding procedures, etc. [3–9]. As a result,
both computational modeling and experimental measure-
ments become much more challenging in dealing with weld
repairs than with initial welds.

Through a careful observation of available residual stress
measurement data and limited 3D finite element modeling
results, certain boundary conditions could be introduced to
approximate some 3D restraint conditions by using a 2D mod-
el. These include generalized plane strain models [2, 5] using

prescribed planar translational and rotational degrees of free-
dom for both plate and pipe components [5–8], and special
composite shell element models [8, 9]. A reasonable estimate
of residual stresses for repair welds has been obtained using
these models with a reduced dimension (see [2, 4, 6–10]), as
demonstrated by comparing finite element results with exper-
imental measurements [10]. These results have showed that
repair weld dimensions are particularly important in contrib-
uting to some residual stress distribution characteristics [6, 7,
13–16] that are of a particular importance to structural integ-
rity. As a result, it has become increasingly apparent that some
of the important residual stress distribution characteristics and
their controlling parameters can be more effectively examined
using rather simple models. As such, basic mechanics associ-
ated with repair weld residual stress generation process can be
more clearly demonstrated. Such an understanding is essential
for establishing a more reliable and consistent scheme for
estimating residual stress profiles for weld repairs in various
components, rather than relying empirical treatment on a case-
to-case basis.

Thus, the purpose of this paper is to establish some impor-
tant features in residual stress distributions uniquely associat-
ed with repair welds and the underlying mechanics, rather
than diving into a detailed discussion on computational and/
or experimental procedures for a particular case of weld repair.
This is because there have been numerous publications in the
literature dealing with detailed repair case studies [1–9],
discussed above. A further emphasis will be placed upon
quantitatively demonstrating the significance of some residual
stress features to structural integrity by comparing crack
growth behaviors in residual stress fields caused by original
fabrication weld and subsequent repair weld, respectively. To
do so, this paper starts a simple 1D (or "one-bar") model
under fully restrained conditions which can be readily solved
analytically to illustrate the basic thermomechanical phenom-
ena involved with a local weld repair. This will be followed by

a three-bar model confirming that fully retrained conditions can be readily achieved in practice under typical repair conditions. These quantitative findings will be used to elucidate the underpinning mechanics associated with some of the residual stress distribution features observed in some early investigations by this and other authors, including implications on structural integrity.

2 Analytical residual stress modeling

The necessary and sufficient conditions for the development of any residual stresses in a component are the presence of localized plastic deformation. Localized plastic deformation in case of welding is resulted from the presence of severe temperature gradients that cause high thermal stresses beyond yield during welding. Such residual stress development process can be effectively demonstrated by an idealized one-dimensional (1D) model (i.e., one-bar model discussed in [13]) in Fig. 2 under fully restrained conditions (Fig. 2a) which can be fulfilled when considering typical weld repair conditions as substantiated in the next section.

2.1 One-bar model

It might be disappointing to some readers that the author has picked a seemingly rather un-impressive residual stress problem and modeling procedure to start with in this paper. Then, the author would like point out here that even with all advanced computational methods and computer power today, a correct finite element solution to such a simple 1D problem in Fig. 2 is not always guaranteed without an adequate

understanding of some of the key thermomechanical phenomena involved. This can be most effectively demonstrated using such a simple 1D problem definition for which analytical solution can be readily developed.

As shown in Fig. 2a, a fully restrained steel bar of unit length at ambient temperature ($\theta = 0$) is assumed subjected to uniform heating, at first linearly increasing over time until reaching to melting temperature ($\theta = \theta_m$), and then linearly decreasing to room temperature (see Fig. 2c). It is further assumed that bar steel follows a stress-strain behavior of elastic perfectly plastic type (see Fig. 2b) with its yield strength (S_Y) as a function of temperature being given in the same figure. Based on incremental plasticity theory, any total measurable strain increment $\Delta\varepsilon$ can be partitioned into strain components as follows, in incremental form:

$$\Delta\varepsilon = \Delta\varepsilon_e + \Delta\varepsilon_p + \Delta\varepsilon_T + \Delta\varepsilon_{Tr} \qquad (1)$$

where $\Delta\varepsilon_e$, $\Delta\varepsilon_p$, $\Delta\varepsilon_T$, and $\Delta\varepsilon_{Tr}$ are elastic, plastic, thermal, and phase transformation-induced strain increments, respectively.

Under fully restrained conditions as shown in the lower part of Fig. 2a, $\Delta\varepsilon = 0$ must be maintained throughout the heating and cooling stages. The resulting strain partitioning in Eq. (1) at any moment in time only depends on the thermomechanical process and what type of strain increments are generated. For instance, at the beginning when temperature is low, there should be only elastic strain $\Delta\varepsilon_e$ present in addition to thermal strain $\Delta\varepsilon_T$; Eq. (2) gives $\Delta\varepsilon_e = -\Delta\varepsilon_T$ or $\Delta\sigma = -\alpha\theta E$ in terms of stress under 1D conditions, as depicted by the shaded area in Fig. 2c. Note that α and E are material's thermal expansion coefficient and Young's modulus, respectively, both of which are assumed to be constant over the entire heating and cooling cycle for simplicity. As

Fig. 2 One-bar model for thermomechanical modeling of residuals stress development process
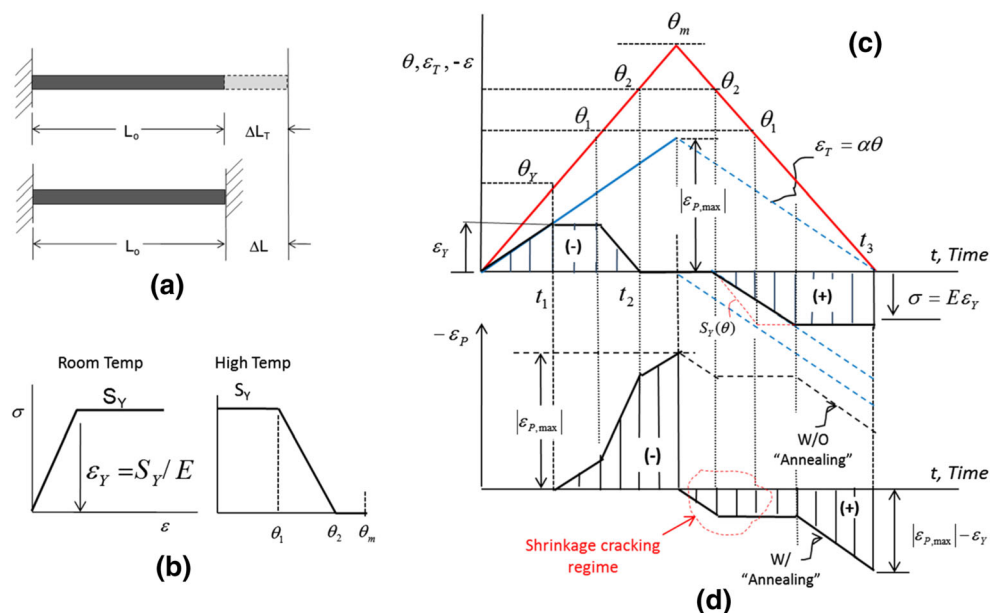
the bar temperature continues increasing, the compressive stress in the bar reaches to the yield strength (S_Y) of the material. At this point, the corresponding compressive elastic strain is at $\varepsilon_Y = S_Y/E$, and the corresponding temperature at yield is $\theta_Y = \varepsilon_Y/\alpha$. To put things in prospective, if one assumes that the bar material is made of low carbon structural steel with the following properties as long as temperature is below θ_1:

$$S_Y = 30 Ksi \quad (207 MPa)$$
$$E = 30 \times 10^3 Ksi \quad (207\ GPa)$$
$$\alpha = 6.5 \times 10^{-6}\ in/in/\mathrm{F}^0 \quad (11.7 \times 10^{-6} mm/mm/C^0)$$

The temperature at yield $\theta_Y(=\varepsilon_Y/\alpha)$ is only about 154 °F (68 °C) under fully restrained conditions. Such conditions are not difficult to achieve when considering a material point near a weld repair.

Further heating beyond θ_Y results in no change in stress or elastic strain until θ_1 is reached. However, the increase in thermal strain with increasing temperature all goes to the equal amount of increase in compressive plastic strain ε_p, as shown in Fig. 2c. A continued increase in temperature from θ_1 to θ_2, material's yield strength decreases linearly with the increase in temperature, approaching nil strength state θ_2. During this time, the development of plastic strain is determined by the difference between the total thermal strain and the elastic strain (shaded region) in Fig. 2d. From θ_2 to θ_m, all thermal strain becomes plastic strain that reaches its maximum shown in Fig. 2d. At $\theta = \theta_m$, the material changes its state from solid to liquid and plastic strain definition ceases to exist, resulting in zero plastic strain ("W/Annealing") or returning to virgin material state upon cooling. This phenomenon is often referred to as numerical "annealing" or "plastic strain annihilation" in finite element modeling context [17]. Otherwise, as shown in Fig. 2c, prior plastic strain history as material passes through melting temperature would have been retained, as shown by the line labeled by "W/O Annealing". Inabilities in dealing with such a melting or remelting phenomena in some earlier publications in literature have been attributed to severe over-estimations in residual stress for materials that exhibit significant strain-hardening.

During the cooling phase starting from θ_m, the decrease in thermal strain can be tracked by translating the line labeled as $\varepsilon_T = \alpha\theta$ vertically down to the zero elastic strain position, which marks the beginning of the shrinkage phase (see Fig. 2d). Due to nil strength of the material, all shrinkage strain becomes plastic strain after θ_m until cooling down to $\theta = \theta_2$. In the context of welding, this is the region that is prone to hot cracking for some materials. The continued tensile plastic strain development can be determined by taking the difference between this line and elastic strain lines enveloping the shaded area in Fig. 2c.

The final residual stress predicted is exactly at yield ($\sigma = S_Y = E\varepsilon_Y$) as shown in Fig. 2c, and plastic strain is tensile and is at $\varepsilon_{p,\ max} - \varepsilon_Y$.

Although the 1D residual stress problem illustrated in Fig. 2 is remarkably simple which was solved graphically, as illustrated in Fig. 1, the results are rather informative, as summarized as follows:

(1) Localized plastic strain can readily develop in welding. As shown in Fig. 2b, a minimum temperature differential $\theta_Y = 154$ °F is sufficient to induce plastic deformation on heating. Furthermore, to generate yield magnitude residual stress in low-carbon steel upon cooling at room temperature, a temperature difference of twice as much, i.e., $2\theta_Y = 308$ °F is all that is needed. Therefore, as far as thermal manufacturing processes are concerned, e.g., thermal forming, cutting, and welding, the presence of residual stresses in fabricated components is commonplace.

(2) For steel types exhibiting strong strain hardening, residual stress components in severely restrained direction (axial direction of bar in this case) can become significantly higher than yield in magnitude, depending upon hardening behavior and the extent of stress triaxiality.

(3) As far as numerical modeling is concerned, the ability to simulate "annealing" effects (annihilation of plastic strain) as material changes its state, e.g., melting, is important, as shown in Fig. 2d. Such an annealing process at a given characteristic temperature also occurs as material goes through phase change in solid state. It must be pointed out that for a given steel material, an accurate determination of the annealing temperature and the extent to which annealing occurs requires sufficient knowledge of material's metallurgical behavior under rapid heating/cooling, which is beyond of the scope of the present discussions.

(4) One additional important observation from the 1D example in Fig. 2 is that to effectively relieve residual stress, the amount of permanent tensile deformation that needs to be introduced into the bar should can be in the order of $\varepsilon_Y (=S_Y/E)$. This only amounts to about 0.001 in permanent strain for this particular case, which can be achieved to a large extent through creep in uniform post-weld heat treatment (PWHT) [18], local mechanical deformation through planishing [2], or other techniques.

Along the same line, general effects of solid-state phase transformation (also referred to as transformation plasticity) on residual stress development can be illustrated. Consider the same bar in Fig. 2a, it may be assumed that the bar material experiences phase change at its first critical transformation occurs, say at θ_2, e.g., a transformation from ferrite to austenite. Such a transformation will be
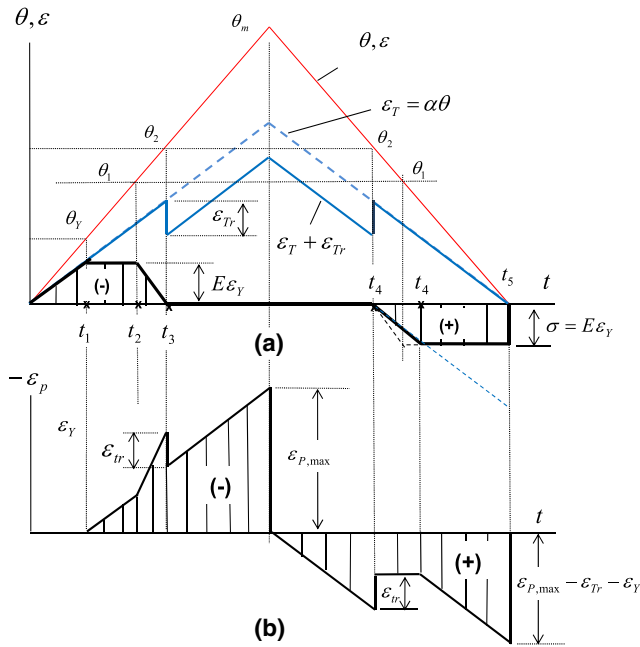
Fig. 3 1D model illustrating phase transformation effects on final residual stress state

accompanied by a volumetric reduction, say in terms of volumetric reduction $\Delta V/V_0$ due to austenite's more compact face-centered cubic (FCC) lattice structure, resulting in an unidirectional strain increment of $\Delta\varepsilon_{Tr} = \frac{\Delta V}{3V_0}$. A reversed transformation in terms of incremental strain at the same temperature on cooling is shown in Fig. 3a. By the following the same graphic solution procedure illustrated in Fig. 2, the elastic strain (ε) or stress ($E\varepsilon$) history is given as the shaded area in Fig. 3a while the plastic strain (ε_p) is shown in Fig. 3b. While plastic strain history clearly indicates the phase transformation effects at high-temperature regime, the resulting residual stress at lower temperature remains the same as the case without considering phase transformation (Fig. 2c). Then, it can be argued that as long as phase transformation plasticity occurs at sufficiently high temperature at which material has a low yield strength, its effects on final residual stresses at room temperature is typically not significant.
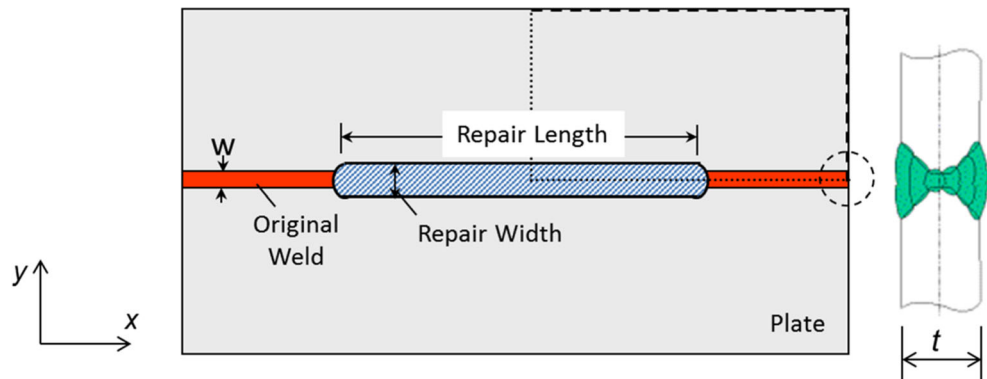
2.2 Three-bar model

A repair weld in a large butt-welded plate is shown in Fig. 4. As discussed in [13], one of the most unique features associated with residual stresses in a weld repair is the fact that there is a significant increase in transverse residual stresses or σ_y, comparing with initial welds. The development of σ_y can be demonstrated by considering a three-bar model with bar orientation in y direction as shown in Fig. 5a, in which bars 1 and 3 model the plate regions outside of the repair length and bar 1 the region within repair length. For simplicity, the areas of bars 1 and 3 are assumed to be the same, i.e., $A_1 = A_2 = A$ which becomes the bar width assuming unity thickness for simplicity. Note that E in Fig. 1 is material Young's modulus of the plate. Upon heating of bar 2, displacement conditions can be described as "plane-remaining-as-plane" or simply as a "rigid link" conditions, as shown in Fig. 5b. These displacement conditions can be written as:

$$\begin{aligned} \delta_1 &= \delta_3 = \delta \quad (Rigid\ link\ and\ symmetry) \\ \delta_2 &= \Delta L_T\text{-}\delta \quad (Deformation\ in\ \text{Bar } 2) \end{aligned} \tag{2}$$

The equilibrium conditions in y can be written as:

$$\begin{aligned} \sum F_y &= 0 \Rightarrow F_1 - F_2 + F_3 = 0 \\ \sum M_2 &= 0 \Rightarrow F_1 d - F_3 d = 0 \end{aligned} \tag{3}$$

Note that bar theory in strengths of materials gives:

$$F_1 = F_3 = \frac{EA\delta}{L_o} \quad and \quad F_2 = -\frac{EA(\Delta L_T - \delta)}{L_o + \Delta L_T}$$

Solving Eqs (2) and (3) leads to:

$$\delta = \delta_1 = \delta_3 = \frac{A_2 \Delta L_T}{2A + A_2} \tag{4}$$
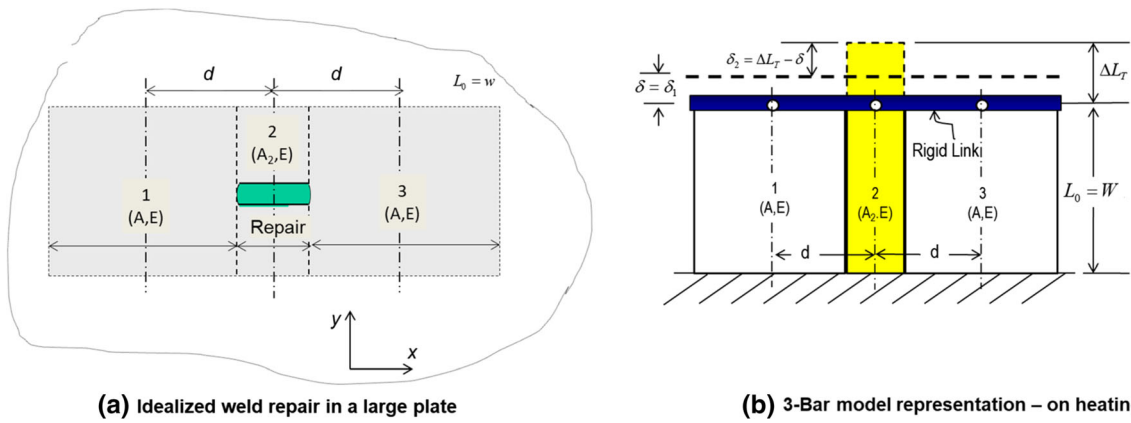
$$\delta_2 = \frac{2A \Delta L_T}{2A + A_2} \tag{5}$$

Fig. 4 A repair weld in a large butt-welded plate

(a) Idealized weld repair in a large plate

(b) 3-Bar model representation – on heating

Fig. 5 a, b Three-bar model based representation of repair weld

in which δ_2 has the largest magnitude while in compression. The corresponding strain can be calculated by simply dividing the displacement by L_0, resulting in:

$$\varepsilon_2 = -\frac{2A\alpha\theta}{2A + A_2}.$$

As temperature in bar 2 continues to rise, the critical temperature differential that leads to yielding in bar 2 can be obtained by setting $\varepsilon_2 = \varepsilon_Y$. For illustration purpose, the following critical θ_Y values can be obtained for different A values:

$$
\begin{aligned}
A &= 2A_2 \Rightarrow \theta_Y = 193\,F \\
A &= 5A_2 \Rightarrow \theta_Y = 169\,F \\
A &\gg A_2 \Rightarrow \theta_Y \to 154\,F
\end{aligned}
\tag{6}
$$

Even at $A = 5A_2$, θ_Y becomes rather close to the value corresponding to $A \gg A_2$. This suggests that the fully restrained conditions as depicted in Fig. 2 can be readily attained in a typical weld repair in an actual component. The resulting thermal stress distribution can be calculated by the equilibrium conditions, i.e.,

$$
\begin{aligned}
\sigma_2 &= -S_Y \\
\sigma_1 &= \sigma_3 = \frac{A_2 S_Y}{2A + A_2}
\end{aligned}
\tag{7}
$$

As discussed in the previous sections, a temperature twice as much, i.e., $2\theta_Y$, is all that is needed to develop yield magnitude residual stress upon returning to room temperature. Beyond $2\theta_Y$, 100% of thermal strain increment contributes to plastic strain increment in compression, which can be shown to be reversed into tensile plastic strain upon cooling at room temperature (see Fig. 2d).

At room temperature, a three-bar model representation of the repair weld shown in Fig. 5a is illustrated in Fig. 6. If the rigid link is not detached, bar 1 and bar 2 would return to their original positions O-O, since there is no plastic deformation occurred in either bar 1 or bar 3 throughout the heating and cooling process. Bar 2 would be shortened

by the amount of $L_0\varepsilon_Y$, since $2\theta_Y$ condition is assumed to be met. The resulting residual stress distribution according to equilibrium condition (now attaching the rigid link) can be calculated in the same manner as in arriving at Eq. (7), as:

$$
\begin{aligned}
\sigma_2 &= S_Y \\
\sigma_1 &= \sigma_3 = \frac{-A_2 S_Y}{2A + A_2}
\end{aligned}
\tag{8}
$$

which gives tensile residual stress of yield magnitude within bar 2 (or repair region) and compressive residual stress outside of the repair region. For a finite size plate, δ_2' represents shrinkage of the three-bar system. Such a residual stress distribution feature (given in Eq. 8) must be present in an actual repair weld. Indeed, Fig. 7 shows the final transverse residual stress distribution in a large thin plate, which was obtained by means of a special shell element modeling procedure with a moving welding heat source being considered [1, 8].

2.3 Some important residual stress features

Residual stresses in repair welds are 3D problems by definition, implying a high degree of complexity in either computational modeling or measurements. However, work to date
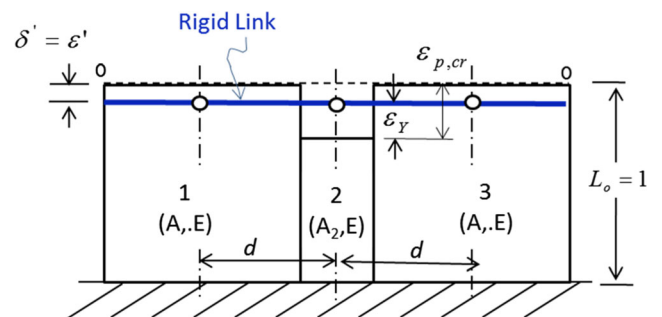

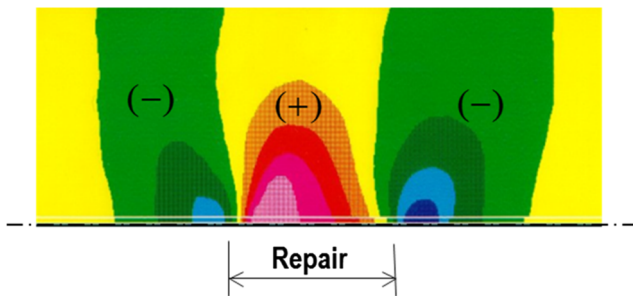**Fig. 6** Three-bar model based representation of repair weld at room temperature

Fig. 7 Transverse residual stress distribution obtained by finite element modeling [1, 7]

suggests that characterization of repair weld residual stresses is not as complicated as initially thought, as it turns out that residual stress distribution characteristics remain similar regardless of component geometric shape, joint type, and material category. This is due to the fact that by definition, majority of repair occurs at a local area and that restraint conditions at local repair is always high regardless of component types. As shown in Fig. 8, transverse residual stresses (perpendicular to repair weld line) in a large aluminum-lithium vessel (Fig. 8a), carbon steel storage tank (Fig. 8b), and stainless steel pipe (Fig. 8c) share rather similar features. Within the repair length, the transverse residual stresses are dominantly tensile at yield strength magnitude for all these cases and become compressive immediately outside of the repair length, suggesting a strong influence of repair length on the extent of such a residual stress distribution. It should be noted that the repairs

considered in Fig. 8 are multi-pass welds, e.g., two passes in Fig. 8a with a repair depth of 0.5t (plate or wall thickness), two passes in Fig. 8b with a repair depth of 0.5, and six passes with a repair depth of 0.8t. Although detailed residual stress distribution tends to vary with respect to number of passes used and repair weld depth, the resulting residual stress distribution characteristics tend to be rather similar. Some specific effects such as effects of repair weld depth will be discussed in the ensuing section.

Indeed, as shown in Fig. 9 for a girth welded stainless pipe, as repair weld length increases, peak transverse residual stress is reduced from peak value of above yield strength magnitude by about 50% for the case of long repair shown in Fig. 9d. Note that finite element modeling results shown in Fig. 9b corresponding to the short repair case were validated by deep hole drilling method [3], as shown in Fig. 10.

Both repair width and length effects are shown in Figs. 10 and 11 for a weld repair in a carbon steel storage tank. An increase in repair width from 1 W to 2 W results in not only an increased peak values in residual stresses, but also in a significant increase in tensile residual stress spread. Note that W represents the initial weld seam width as shown in Fig. 4. Effects of repair length are consistent with those observed in Fig. 9 in a pipe girth weld.

Figure 12 shows repair depth effects on residual stress distributions for a pipe girth weld. As can be seen, as repair depth increases, high tensile residual stresses develop into pipe wall thickness, particularly at inner surface.
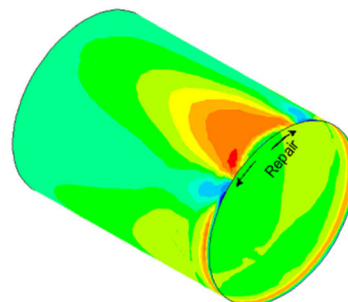
Fig. 8 a–c Transverse (to repair weld) residual stress distributions in three different components made of various material types
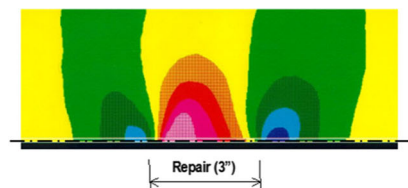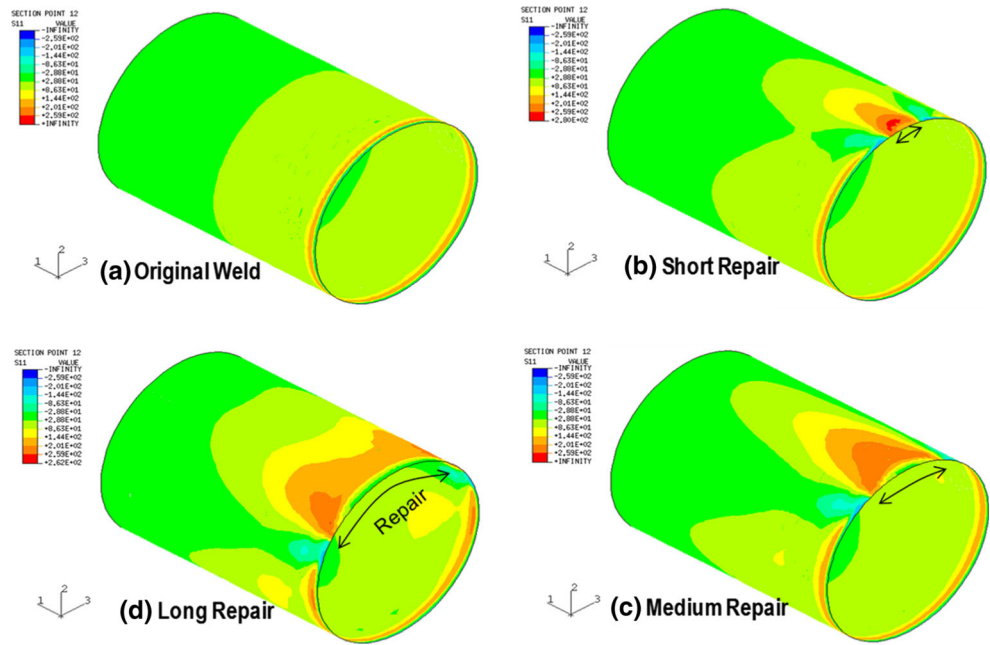

(a) Repair of a butt weld in AL 2195 plate
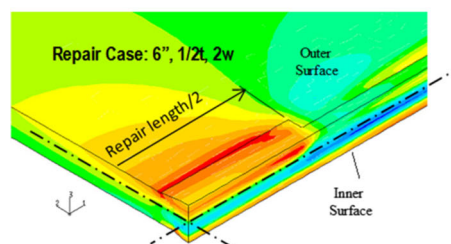
(b) Repair of longitudinal butt weld in carbon steel storage tank

(c) Repair of girth weld in a stainless Steel Pipe

Fig. 9 **a–d** Effects on repair length on transverse residual stresses—a repair along girth weld of a stainless steel pipe

(a) Original Weld

(b) Short Repair

(d) Long Repair

(c) Medium Repair

3 Significance to structural integrity

3.1 Fracture mechanics treatment of residual stresses

As an example, at a first glance at Fig. 12, the differences in through-thickness residual stress distributions seem somewhat subtle with an overall elevation of tensile residual stresses across pipe wall thickness as repair

depth increases. To facilitate a quantitative comparison, a through-thickness residual stress decomposition technique [15] is adopted here, since such a technique also enables a direct comparison in terms of fracture driving force, e.g., stress intensity factor (K) caused by residual stresses. For a given through-thickness residual distribution such as those shown in Fig. 12, say at weld toe, it can be decomposed into three parts: through-thickness
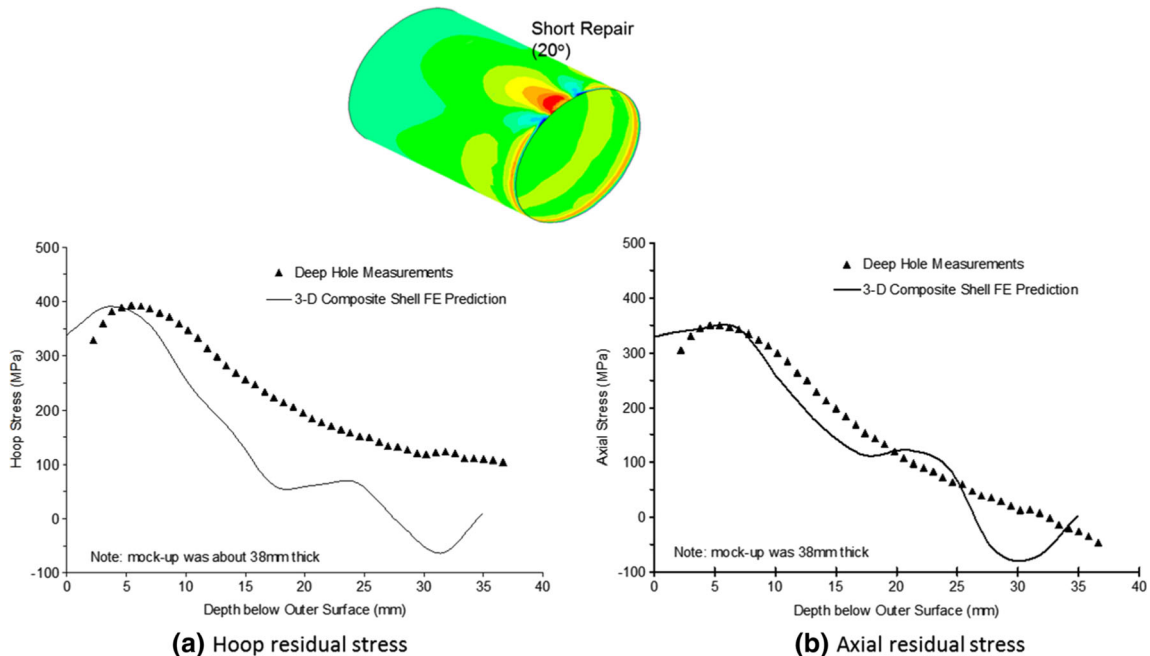

(a) Hoop residual stress

(b) Axial residual stress

Fig. 10 **a, b** Comparison of through-wall residual stresses in the HAZ at mid-length of a short 20° arc repair—measurements versus modeling results
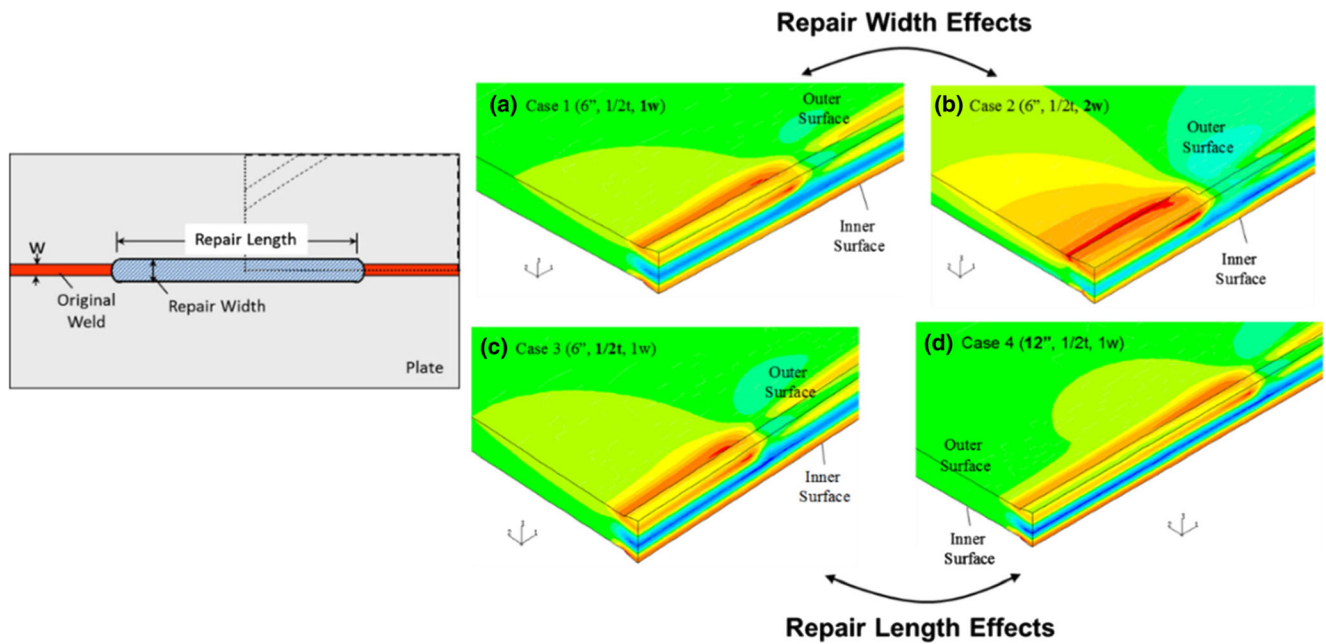
Fig. 11 Transverse residual stresses in repair weld in carbon steel storage tank: effects of repair width and repair length

membrane (σ_m), bending (σ_b), and self-equilibrating ($\sigma_{s.\ e}$), as:

$$\sigma_{\mathrm{m}} = \frac{1}{t} \int_0^t \sigma(x)dx$$

$$\sigma_{\mathrm{b}} = \frac{6}{t^2} \int_0^t \sigma(x)\left(x - \frac{t}{2}\right)dx \qquad (9)$$

$$\sigma_{\mathrm{s.e.}} = \sigma(x) - \sigma_{\mathrm{m}} - \sigma_{\mathrm{b}}\left(1 - \frac{2x}{t}\right)$$

where x is measured from pipe inner surface or ID and t is component wall thickness. As discussed in [15], the three parts given in Eq. (9) have rather different contributions to fracture driving force, with the membrane part (σ_m) being the most important, followed by the bending part (σ_b), and the self-equilibrating part being the least important. By considering only the through-thickness membrane and bending parts in Eq. (9), the results after decomposition are shown in Fig. 13. Now, it can be clearly seen that as repair depth increases from 0.2t to 0.6t, through-thickness membrane stress rapidly increases while through-thickness bending stress decreases.

As discussed by Dong [15], through-thickness membrane stress has a dominant effect in stress intensity factor for a growing crack in residual stress field. By considering both through membrane and bending stresses, the stress intensity factor solution following the displacement-controlled technique in [15] is shown in Fig. 14 assuming that a circumferential crack is situated at weld toe position at either pipe outer surface or inner

Fig. 12 Repair depth effects on hoop and axial residual stress distributions in a girth welded pipe (repair length 20°angular span; repair width 1 W; $r/t = 12$)
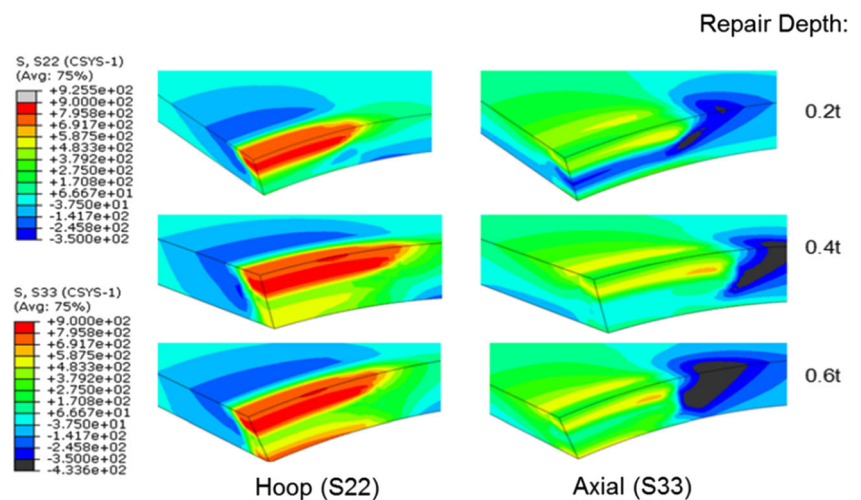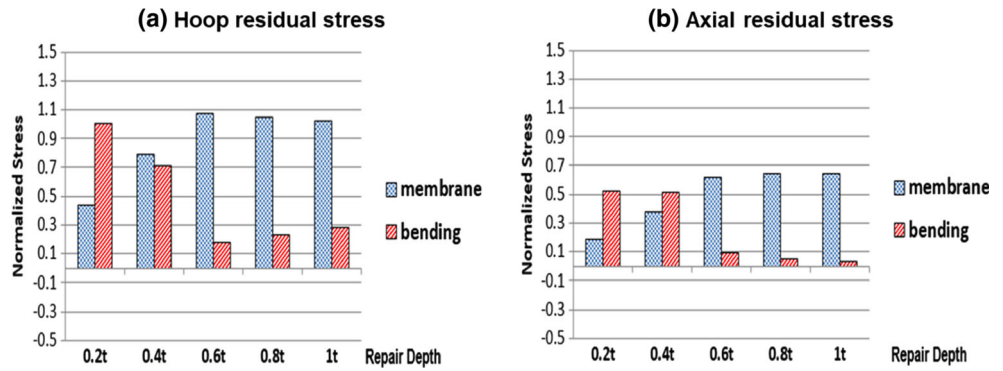
(a) Hoop residual stress

(b) Axial residual stress

surface. Note that, as discussed in [15], the displacement-controlled K solution enables a consideration of residual stress relaxation effects on K as a crack extends. In both cases, a shallower repair (say at 0.2t) tends to generate a much lower K as a function of crack size than a deeper repair (say at 0.6t) for a crack situated either at OD (Fig. 14a) or ID (Fig. 14b).

3.2 Elliptical surface crack

In the previous section, circumferential cracks situated in repair weld residual stress fields corresponding to various depths of weld repairs in a pipe girth weld are considered. Small elliptical surface crack behaviors in a repair weld in girth weld in a large diameter storage tank (see Fig. 11) are investigated here, at which stress corrosion cracking had been found and potential crack growth under continued service is of particular interest [18]. Two hypothetical surface crack configurations (one parallel and one transverse to weld) are examined here for the repair case shown in Fig. 11 with a repair length of 6″, depth of 0.5t, and width of 2 W. Note that in this particular instance, applied load is negligible. As a result, only stresses that are possibly operative can be attributed to residual stresses due to welding either from original weld or repair weld. Figure 15 shows the stress intensity factor distributions along a surface crack (length of 2a along surface and c in depth) situated in the HAZ (parallel to weld line) by assuming a self-similar growth. The stress intensity results are plotted

against elliptical angle with 0° being defined at surface and 90° being at the deepest point (Fig. 15a). The significant increase in stress intensity factor for all crack sizes considered is evident due to the presence of repair (Fig. 15b). At the original weld without any weld repairs, the parallel surface crack is unlikely to break through the inner surface (wall thickness of $0.625''$) since as the crack depth is increased to $c = 0.3''$ with corresponding half crack length $c = 0.6''$, stress intensity factor K becomes negative at about 90° (Fig. 11a) In contrast, K still remains high and stay positive at $a = 0.8''$ and $c = 0.4''$ (Fig. 15b). For a transverse crack on which the longitudinal residual stresses will be operative, the significant increase in for all crack sizes due to repair can also be seen in Fig. 16.

In recognizing the detrimental effects on residual stresses in weld repairs, repair weld dimensions should be carefully considered as an essential part of the residual stress mitigation strategy as discussed in Section 2.3. Although conventional uniform post-weld heat treatment (PWHT), e.g., placing an entire component in a furnace, is effective as recently investigated by Dong et al. [17], its implementation can be often difficult when dealing with operating equipment, for which local PWHT through a local heating may be the only option available. Unfortunately, such a local PWHT can be rather tricky to use, more often than not causing additional residual stresses due to significant thermal stresses generated by the local PWHT process [19] and restraints by surrounding structure, which can lead to complex deformation patterns in curtain pipe and vessel components. These
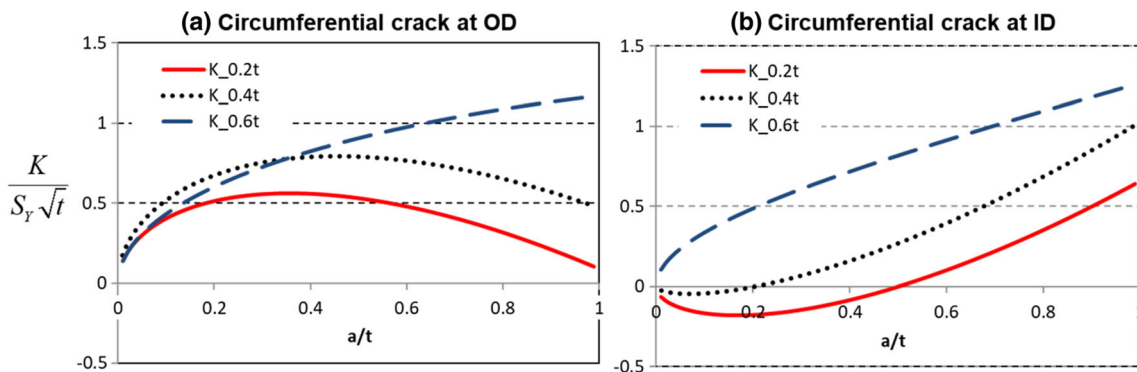

(a) Circumferential crack at OD

(b) Circumferential crack at ID

Fig. 14 Comparison of normalized stress intensity factor ($K/S_Y\sqrt{t}$) as a function of relative crack size (a/t) for a hypothetical circumferential crack situated at weld toe caused by axial residual stress only (i.e., no applied external load)—repair depth effects **a** cracking at OD and **b** cracking at ID
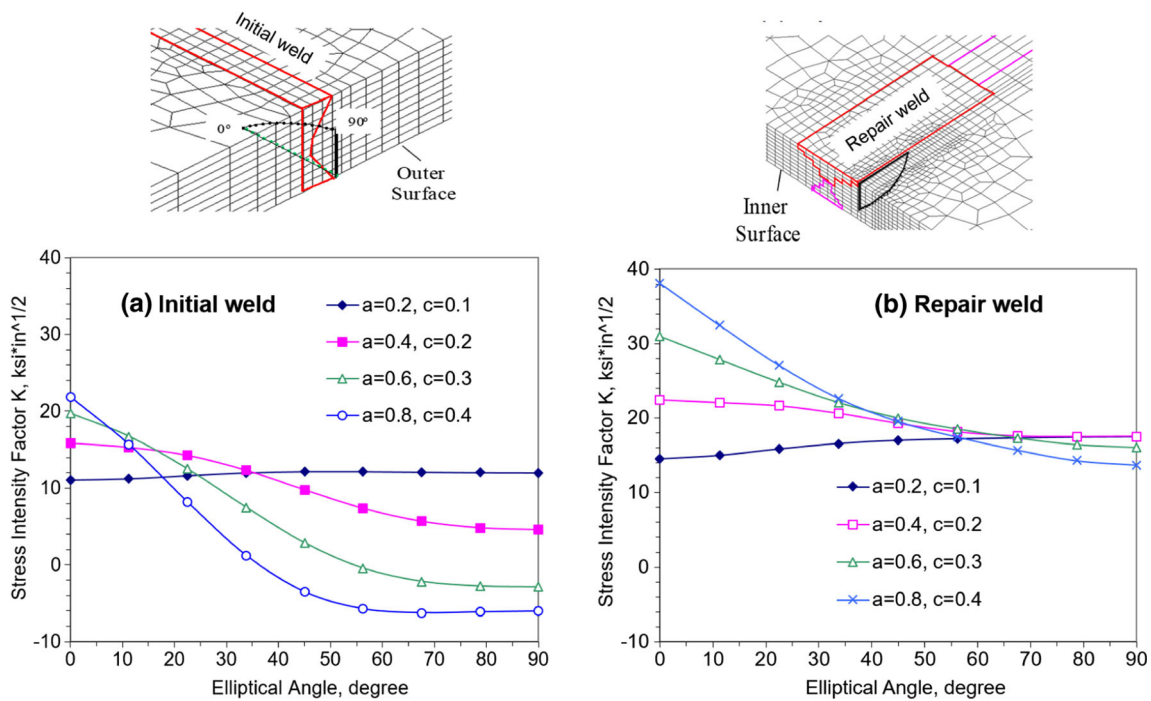
Fig. 15 a, b Comparison of stress intensity factor (K) solutions for a growing parallel surface crack along weld toe

components are often associated with a large component radius to wall thickness ratio (or r/t), in which through-wall axial residual stress distributions typically exhibit a self-equilibrating type (see recent results given in [19–21] for girth welds and in [22, 23] for longitudinal seam welds by using a weld material constitutive model similar to the one described in [24]). Any weld repairs

on this type of components will significantly increase through-thickness membrane and bending components, as shown in Fig. 11, on which local PWHT has been shown very difficult. As a result, a proper consideration of repair weld dimensions can be very beneficial for reducing repair-induced residual stresses, rather than resorting local PWHT. As demonstrated in the
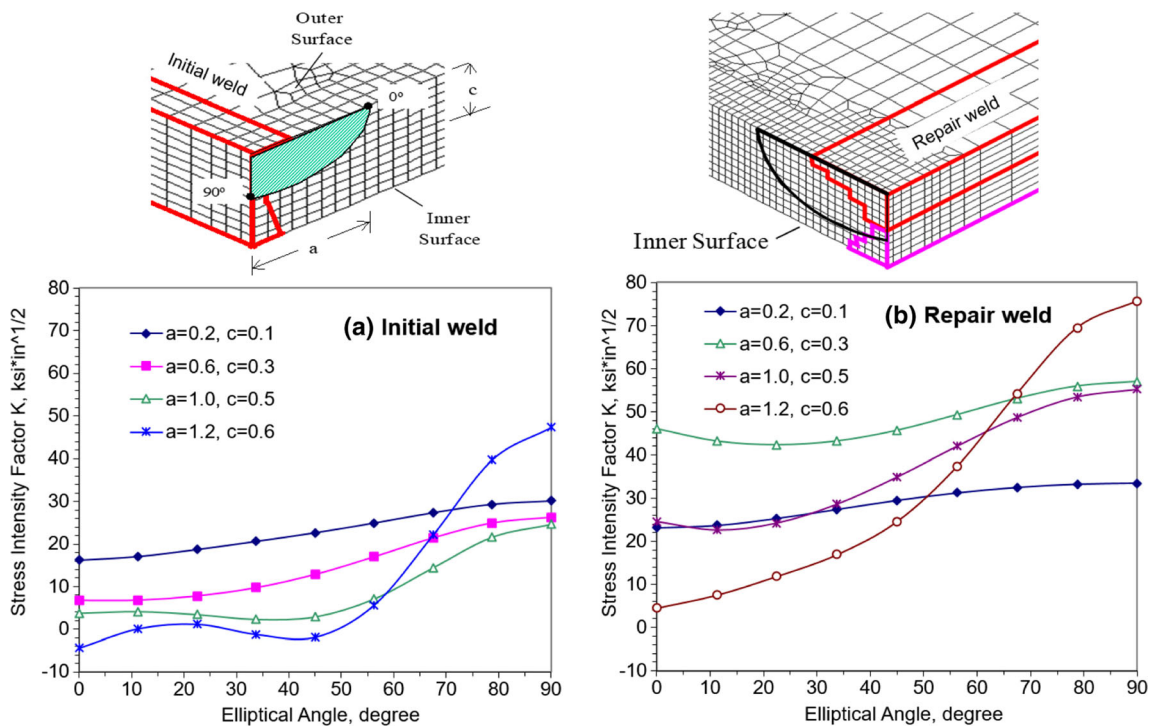

Fig. 16 a, b Comparison of stress intensity factor (K) for a growing transverse surface crack

previous section and this section, a desirable repair weld dimensions should be as long as possible, as shallow as possible, and as narrow as possible.

4 Concluding remarks

As quantitatively demonstrated by the one-bar and three-bar analytical models presented in this paper, weld repairs are subjected to almost equally high restraint conditions in both transverse and longitudinal directions with respect to weld, while in original welds, high restraint conditions typically occur in the longitudinal direction or parallel to weld. Such unique restraint conditions associated with weld repairs produce some invariant stress distribution characteristics that can be observed regardless of component geometries, materials, and welding procedures as long as repair size is small comparing with overall component dimensions. One major detrimental effect of a weld repair on structural integrity is its elevated membrane stress level, resulting in significantly increased fracture driving force, e.g., stress intensity factor (K) for a hypothetical crack situated either in transverse and longitudinal direction of a repair weld. One effective means for reducing membrane stress is through a proper sizing of a weld repair if possible. As demonstrated in this paper, a preferred repair weld geometry should be as shallow as possible, as narrow as possible, and as long as possible, rather than based on defect size and shape to be repaired.

References

1. Dong P, Hong JK, Rogers P (1998) Analysis of residual stresses in Al-Li repair welds and mitigation techniques. Welding J Res Supplement 77:439-s

2. Dong P, Hong JK, Zhang J, Rogers P, Bynum J, Shah S (1998) Effects of repair weld residual stresses on wide-panel specimens loaded in tension. J Press Vessel Technol 120(2):122–128. https://doi.org/10.1115/1.2842229

3. George, D., Smith, D.J., and Bouchard, P.J. (1999) Evaluation of through wall residual stresses in stainless steel repair welds, Proc. Fifth European Conference on Residual Stresses (ECRS5) Delft-Noordwijkerhout, The Netherlands

4. Bouchard PJ, George D, Santisteban JR, Bruno G, Dutta M, Edwards L, Kingston E, Smith DJ (2005) Measurement of the residual stresses in a stainless steel pipe girth weld containing long and short repairs. Int J Press Vessel Pip 82(4):299–310. https://doi.org/10.1016/j.ijpvp.2004.08.008

5. Dong P, Brust FW (2000) Welding residual stresses and effects on fracture in pressure vessel and piping components: a millennium review and beyond, The Millennium Issue, ASME Transactions. J Press Vessel Technol 122(3):329–328. https://doi.org/10.1115/1.556189

6. Dong P, Zhang J, Bouchard PJ (2002) Effects of repair weld length on residual stress distribution. J Press Vessel Technol 124(1):74–80. https://doi.org/10.1115/1.1429230

7. Dong P, Hong JK, Bouchard PJ (2005) Analysis of residual stresses at weld repairs. Int J Press Vessel Pip 82(4):258–269. https://doi.org/10.1016/j.ijpvp.2004.08.004

8. Zhang, J., Dong, P., and Brust, F.W. (1997) A 3-D composite shell element model for residual stress analysis of multi-pass welds, Transactions of the 14th International Conference on Structural Mechanics in Reactor Technology (SMiRT 14), Lyon, France, Vol. 1, pp. 335–344

9. Dong P (2001) Residual stress analyses of a multi-pass girth weld: 3-D special shell versus axisymmetric models. J Press Vessel Technol 123(2):207–213. https://doi.org/10.1115/1.1359527

10. BS7910:2013 (2013) Guide to Methods of Assessing the Acceptability of Flaws in Metallic Structures. British Standards Institution, London

11. EDF Energy (2015) R6: assessment of the integrity of structures containing defects, Revision 4, with amendments to Amendment 11, Gloucester

12. American Petroleum Institute/ASME (2007) Fitness-for-Service, API 579-1/ASME FFS-1, Washington DC

13. Dong P (2014) Residual Stresses in Weld Repairs. In: Hetnarski RB (ed) Encyclopedia of Thermal Stresses. Springer, Dordrecht

14. Song S, Dong P (2016) Residual stresses at weld repairs and effects of repair geometry. Sci Technol Weld Join 22(4):265–277. https://doi.org/10.1080/13621718.2016.1224544

15. Dong P (2008) Length scale of secondary stresses in fracture and fatigue. Int J Press Vessel Pip 85(3):128–143. https://doi.org/10.1016/j.ijpvp.2007.10.005

16. Dong P, Song S, Zhang J, Kim MH (2014) On residual stress prescriptions for fitness for service assessment of pipe girth welds. Int J Press Vessel Pip 123:19–29

17. Brust FW, Dong P, Zhang J (1997) A constitutive model for welding process simulation using finite element methods. In: Atluri S, Yagawa G (eds) Advances in Computational Engineering Sciences. Tech Science Press, Anaheim, pp. 51–56

18. Dong P, Song S, Zhang J (2014) Analysis of residual stress relief mechanisms in post-weld heat treatment. Int J Press Vessel Pip 122:6–14. https://doi.org/10.1016/j.ijpvp.2014.06.002

19. Dong P, Song S, Pei X (2016) An IIW residual stress profile estimation scheme for girth welds in pressure vessel and piping components. Weld World J 60(2):283–298. https://doi.org/10.1007/s40194-015-0286-4

20. Song S, Dong P, Pei X (2015) A full-field residual stress estimation scheme for fitness-for-service assessment of pipe girth welds: Part II–A shell theory based implementation. Int J Pres Vess Pip 128(4/30):8–17

21. Song S, Dong P, Pei X (2015) A full-field residual stress estimation scheme for fitness-for-service assessment of pipe girth welds: Part I—Identification of key parameters. Int J Press Vess Pip 126-127(1/20):58–70

22. Song S, Dong P (2016) A framework for estimating residual stress profile in seam-welded pipe and vessel components part I: weld region. Int J Press Vessel Pip 146:74–86. https://doi.org/10.1016/j.ijpvp.2016.07.009

23. Song S, Dong P (2016) A framework for estimating residual stress profile in seam welded pipe and vessel components part II: outside of weld region. Int J Press Vessel Pip 146:65–73. https://doi.org/10.1016/j.ijpvp.2016.07.010

24. Ashok N, Dong P, Zhang J, Brust F, Dong Y (2004) Method for determining a model for a welding simulation and model thereof, US Patent 6,768,974s